Applied Surface Science 492 (2019) 328–336

Contents lists available at ScienceDirect

Applied Surface Science

journal homepage: www.elsevier.com/locate/apsusc

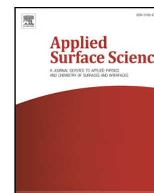

Full length article

# Layered $Al_2O_3$-$SiO_2$ and $Al_2O_3$-$Ta_2O_5$ thin-film composites for high dielectric strength, deposited by pulsed direct current and radio frequency magnetron sputtering

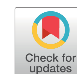

Benjamin V.T. Hanby[a,*], Bryan W. Stuart[a], Miquel Gimeno-Fabra[a], Jonathan Moffat[b], Chris Gerada[c], David M. Grant[a,*]

[a] Advanced Materials Research Group, Faculty of Engineering, University of Nottingham, NG7 2RD, UK
[b] Oxford Instruments, Asylum Research, High Wycombe HP12 3SE, UK
[c] Department of Electrical and Electronic Engineering, University of Nottingham, NG7 2RD, UK

A R T I C L E I N F O

*Keywords:*
Magnetron sputtering
Multilayers
Dielectric strength
Adhesion
Insulation

A B S T R A C T

Multilayer thin films have the potential to act as high dielectric strength insulation for wire and microelectronics. In this study, films consisting of 2, 4 or 8 layers, composed of $Al_2O_3$ with $SiO_2$ or $Ta_2O_5$, were prepared *via* pulsed direct current and radio frequency magnetron sputtering to a thickness of between 152 and 236 nm. The dielectric strengths of all films exceeded the 310 $V\mu m^{-1}$ achieved for PDC $Al_2O_3$. Maximum dielectric strengths were obtained for four layer composites; $Al_2O_3$-$SiO_2$-$Al_2O_3$-$SiO_2$ (466 $V\mu m^{-1}$) and $Al_2O_3$-$Ta_2O_5$-$Al_2O_3$-$Ta_2O_5$ (513 $V\mu m^{-1}$), each containing two PDC-$Al_2O_3$ and two RF-$SiO_2$/$Ta_2O_5$ layers. Whilst the average dielectric strength was higher in the $Ta_2O_5$ composites, they suffered from higher leakage prior to breakdown with *ca.* 6.5 nA compared to *ca.* 0.1 nA for $SiO_2$ composites. The mechanical properties of the composites were poorer due to increased intrinsic coating stress. Samples exhibited complete interfacial delamination with maximum coating adhesion strengths of 22 and 25 MPa. The variance resulted from larger coefficient of thermal expansion for $Ta_2O_5$ compared to $SiO_2$. Sputtered composites of $Al_2O_3$ and either $SiO_2$ or $Ta_2O_5$ had high breakdown strength with reasonable adhesion and could be suitable for insulating copper conductors in the aerospace and automotive industries.

## 1. Introduction

Highly insulating ceramic films are of great interest as dielectric layers in microelectronics for thin-film capacitors and field effect transistors [1,2]. Furthermore, thin high-strength dielectric films offer a route to improve packing densities in wire insulation and are desirable in aviation and automotive applications, where a drive for electrification is pushing for the improvement of all aspects within electrical systems. As such, lightweight, thermally stable and high breakdown strength insulation is required for windings in motors and actuators [3]. An airbus A3800–800 contains *ca.* 470 km of wire with a total weight of 5700 kg. The electrical insulation commonly consists of PTFE/polyimide/PTFE composites, because of its arc track resistance, compared to polyimide alone and maximum operating temperature of *ca.* 260 °C [4,5]. With the further evolution of more electrical aircraft the amount of wire used is bound to increase, whereby improvements in dielectric strength/ thermal stability of the insulation could be used to reduce the weight and space taken up by the total wire [3].

Physical Vapour Deposition (PVD) techniques such as magnetron sputtering have been shown to be capable of producing alumina films with dielectric strength as high as 1.5 $kV\mu m^{-1}$, such as those produced by *Carreri*et al. when using special power supplies to pulse the Direct Current (PDC) power and quench arc events [6–8]. Further to these desirable electrical properties PDC alumina films are considered a suitable base material for electrically insulating multilayer composites as they have been shown to adhere well to copper, exhibiting pull off adhesion values of up to 56 MPa and have deposition rates up to 76 $nmh^{-1}$ with sample rotation [8]. Sputtering is also attractive because the thin films it deposits can be tailored to prevent cracking and delamination, namely by monitoring thickness and mitigating thermal expansion variation and high internal stress [9,10].

Multilayer materials have been used as a route to combine desirable material properties, such as in ceramic capacitors where multilayers improve electrical properties including dielectric constant and

* Corresponding authors.
*E-mail addresses:* Benjamin.hanby@nottingham.ac.uk (B.V.T. Hanby), David.grant@nottingham.ac.uk (D.M. Grant).

https://doi.org/10.1016/j.apsusc.2019.06.202
Received 29 April 2019; Received in revised form 18 June 2019; Accepted 20 June 2019
Available online 21 June 2019
0169-4332/ © 2019 The Authors. Published by Elsevier B.V. This is an open access article under the CC BY license (http://creativecommons.org/licenses/by/4.0/).

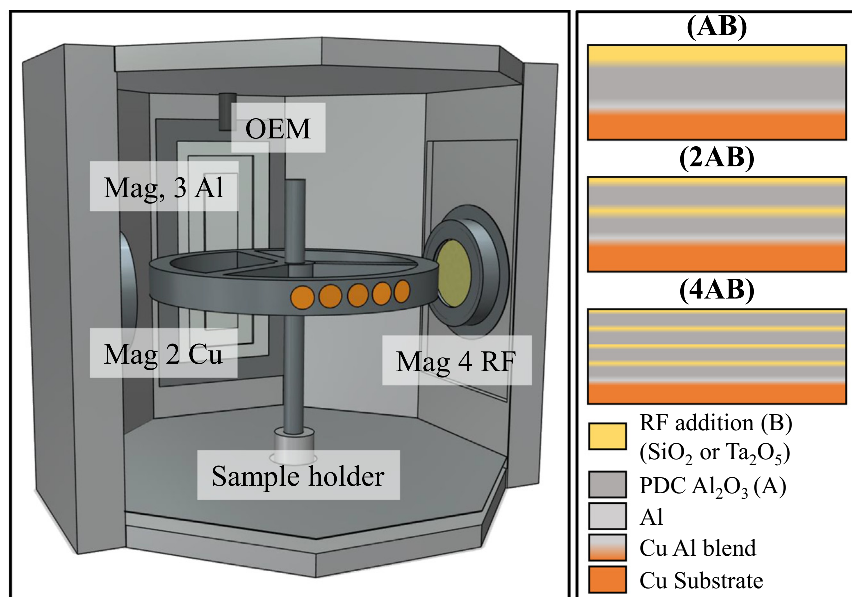


**Fig. 1.** TEER UDP-650 front on configuration with targets in Mag 2 (RF Cu), Mag 3 (PDC Al) and Mag 4 (RF $SiO_2$ or RF $Ta_2O_5$). The OEM is located above mag 3 and is used to control plasma intensity of the Al target used to prepare multilayer PDC alumina materials with a blended copper aluminium interlayer. On the right is a summary of the nomenclature used to refer to the $Al_2O_3$-$Ta_2O_5$ and $Al_2O_3$-$SiO_2$ composites produced in this study (where A refers to PDC alumina and B refers to the RF addition $SiO_2$ or $Ta_2O_5$).

dielectric strength, by introducing barriers to current flow and defect filling [11–13]. It is important to consider barrier layer thickness, as shown by *Chu and Shen* where increasing the number of layers from 174 to 800 in TiN/TiBN films was shown to result in a 50% reduction in hardness and a 79% reduction in adhesive scratch failure [14]. Film doping is another potential route to improving the dielectric strength of sputtered ceramics; for instance a 10 mol% lanthanum inclusion was shown to increase the dielectric strength of sol-gel $Al_2O_3$ films from 310 to 393 $V\mu m^{-1}$ and reduce leakage current three fold, as shown by *Zou* et al. [15]. However, multilayers are more appropriate because of the higher level of consistency attainable, because of issues with complex preferential sputtering and target erosion during sputtering from compound and composite targets when doping [16]. Preferential sputtering is caused by the varying sputtering yields of elements in a compound target, which results in a coating composition which differs from the target [17].

$SiO_2$ is an attractive option for use in multilayer materials and it has been sputtered using various power supply options from Si or $SiO_2$ targets. Films deposited using reactive radio frequency (RF) sputtering by *Jun* et al. achieved good dielectric strengths up to 570 $V\mu m^{-1}$, higher than that of sputtered alumina films produced in previous work [18,19]. However, these RF sputtered films suffer from low deposition rate, for example *ca.* 300 $nmh^{-1}$ without sample rotation, making them impractical from a fabrication standpoint. Multilayer films consisting of sputtered $Al_2O_3$ and $SiO_2$ produced by *Martínez-Perdiguero* et al. showed a two fold increase in dielectric strength when comparing the electrical properties to those of $Al_2O_3$ alone [20]. Also displaying a maximum dielectric strength of > 160 $V\mu m^{-1}$ for an annealed 8 layer structure. Improvements in this case were attributed to structure stabilisation. $Al_2O_3$-$SiO_2$ multilayer materials have also been studied for gas diffusion barriers as produced by atomic layer deposition and sputtering [13,21]. These multilayers have found such application because of subsequent layers ability to close pinhole defects. In the case of electrical insulating films this effect would also be beneficial.

$Ta_2O_5$ is another ceramic which has often been utilised in the electronics industry, as a material with a very high dielectric constant of up to 23, therefore, it is a highly attractive material for thin film capacitors among other applications [22]. $Ta_2O_5$-thin films have been frequently deposited using various techniques as discussed by *Chaneliere* et al. [23]. Deposition of films using RF sputtering has been able to produce materials with high dielectric strength, such as 400 $V\mu m^{-1}$ achieved by *Oehlein* et al. and 600 $V\mu m^{-1}$ for *ca.* 60 nm films deposited by *Seki* et al. [24,25]. $Ta_2O_5$ $Al_2O_3$ nano laminates have been produced using ALD by *Smith* et al. [26]. These ALD composites were produced as films for capacitors and to have a high dielectric constant between 8.9 and 23.9 for pure $Al_2O_3$ and $Ta_2O_5$ respectively. Their work showed that the layered films exhibited lower leakage current values than $Al_2O_3$ alone over certain applied voltage ranges.

Dielectric properties have been reported for layered magnetron sputtered $Al_2O_3$-$SiO_2$ composites. However, reports are lacking for layered magnetron sputtered $Al_2O_3$-$Ta_2O_5$ composites and further elucidation is required to fully understand the mechanisms by which incorporating multilayers improves the dielectric strength in both material systems [20,26]. A more substantial assessment of the effect of the number of layers and the layer thickness would also aid in the future design of high performance ceramic multilayers to increase the dielectric strength and adhesion strength. Further to this it is noted that AFM breakdown methods have not been used to measure the properties of composite materials with such thickness, which is usually limited to ultra-thin films and it is important to show the methods applicability [27–29].

The aim of this study is to utilise the potential of multi-layered ceramic films, based upon pulsed direct current sputtered $Al_2O_3$ with either RF sputtered $Ta_2O_5$ or $SiO_2$ to improve the dielectric strength of the single layer $Al_2O_3$ films as previously deposited [8]. The combination of PDC and RF sputtering is proposed in order to utilise the high quality of RF films and the higher deposition rates of PDC deposition whilst also facilitating blending to prevent cohesive failure and limiting the requirements for multiple optical emission monitoring (OEM) systems. All of this is carried out in order to produce the next generation of thermally stable, high breakdown strength insulators, which maintain adhesive properties to copper substrates.

## 2. Methodology

### 2.1. Coating and sample preparation

Cu disk substrates of 5 and 10 mm diameter with a thickness of 2 mm were punched from Cu sheet (Cu-CW004A-H065 of 99.9% purity) and were polished using sequentially higher grit silicon carbide grinding and polishing papers (240 to 4000 Grit) with water as a lubricant. Followed by colloidal silica polishing (particle size of 0.06 μm) using an MD-Chem polishing pad (Struers®). Samples were then ultrasonicated for 10 min each in acetone and ethanol. Coatings were

**Table 1**
Alumina coating parameters for the multilayer composite films. Note the time used for RF stages ($Ta_2O_5$ or $SiO_2$) excluded the 15 min ramp stages prior and post layer formation. The initial PDC layer was followed with either RF $Ta_2O_5$ or RF $SiO_2$ depending on the type of composite being produced.

| Layer config. | PDC $Al_2O_3$ per layer (min) | RF $Ta_2O_5$ per layer (min) | RF $SiO_2$ per layer (min) | RF target power (W) | Ar Gas Flow (sccm) | Pulse Freq. (kHz) | Duty Cycle (%) |
|---|---|---|---|---|---|---|---|
| AB | 133.3 | 30.9 | 155.4 | 100 | 140 | 150 | 40 |
| 2AB | 66.7 | 15.0 | 77.2 | 100 | 140 | 150 | 40 |
| 4AB | 33.3 | 7.2 | 38.6 | 100 | 140 | 150 | 40 |

deposited in a TEER UDP-650 magnetron sputtering rig (see Fig. 1 for sputtering rig layout and magnetron placement). Al targets were pre-cleaned until the optical emissions monitoring (OEM) plasma intensity returned to that of the un-poisoned target. Optical emission monitoring and optimisation has been discussed previously and is used to control the flow of reactive gas, in order to deposit stoichiometric materials [8]. The optical emissions monitoring system monitors the intensity of the plasma and is calibrated when sputtering in 100% argon, the reactive gas is then added until the intensity is decreased to a desired set point. An OEM set point of 23% was used to deposit $Al_2O_3$ from an Al target in this study. The Cu target (mag 2 – Fig. 1) was pre-cleaned for 10 min at 60 W. RF targets (mag 4 - Fig. 1) were pre-cleaned for a total of 15 min with a 5 min power ramp up stage, so as not to damage the target.

Films were sputtered to a total thickness of *ca.* 200 nm with a varying number of layers. Alternate layers of pulsed DC $Al_2O_3$ (allocated A) and RF $SiO_2$ or RF $Ta_2O_5$ (the added RF layer is allocated B) were deposited so as to form AB, ABAB (2AB) and ABABABAB (4AB) composites as seen in Fig. 1 using deposition parameters as shown in Table 1.

$Al_2O_3$ layers were sputtered using pulsed direct current sputtering according to films as produced by in a previous study, with a blended Cu/Al interlayer [8]. The Al interlayer was deposited using PDC power at 4 A as opposed to 6 A DC as used in the previous study. This was primarily done to achieve stable arc free deposition. Sputtering times were used as in Table 1 in order to deposit a film of *ca.* 200 nm total thickness, containing *ca.* 150 nm of pulsed DC $Al_2O_3$. Note that RF magnetrons were allowed to ramp for 15 min prior to the time given in Table 1 and also allowed 15 min to ramp to 0 following each layer, creating the blended interfaces.

### 2.2. Characterisation

#### 2.2.1. Fourier transform infrared spectroscopy

Fourier Transform Infrared Spectroscopy (FTIR) was carried out using a Bruker Tensor FTIR instrument. An Attenuated Total Reflectance (ATR) attachment with a diamond mirror and ZnSe lens was used to measure sample IR absorbance between 500 and 1500 $cm^{-1}$ wavenumbers. A resolution of 4 $cm^{-1}$ was used.

#### 2.2.2. XRD

X-ray Diffraction (XRD) was carried out using a Bruker D8 Advanced diffractometer. A glancing angle of 1.2° was applied with a step size of 0.04° and a counting time of 20 s, scanning between 2θ values of 15 and 80°. Diffraction patterns were analysed using Bruker's EVA software.

#### 2.2.3. XPS

X-ray photoelectron spectroscopy (XPS) was used to determine the elemental composition of the top surface (*ca.* 5 nm) of the material [30]. Samples were analysed in an ESCA lab mark II with an Al Kα non-monochromatic X-ray source at $< 10^{-7}$ Torr. A survey spectra was collected from two scans between 0 and 1200 eV with a step size of 1.0 eV and a dwell time of 0.2 s. Five high resolution scans of O_1S, C_1S and either Ta_4F or Si_2P were averaged with a step size of 0.2 eV and a dwell time of 0.4 s. Charge shift correction was applied to all spectra through calibration with the C_1S peak using the ideal value of 284.8 eV.

#### 2.2.4. SEM

Coated copper samples were mounted in resin perpendicular to the normal to obtain polished cross section as in Section 2.1. Samples were ultra-sonicated and iridium coated (*ca.* 8 nm) using a Q150R Plus coater. Samples thickness and structure were determined using A JEOL 7100F Field Emission Gun Scanning Electron Microscope (FEG-SEM) operating at 15 kV, with a working distance of 10 mm.

### 2.3. Mechanical testing

#### 2.3.1. Pull off testing

In accordance with ASTM-D4541–09 DFD E1100S epoxy was applied to a cleaned 2.8 mm diameter stub and pressed onto a 10 mm diameter coated Cu disk. The stub was pressed down to remove any air and then cured on a heating plate for 1 h at 140 °C. Once cured any excess glue from around the stub was removed with the supplied cylindrical cutting tool. The samples were tested with a DFD instruments P.A.T. handy pull off adhesion unit and adhesion strength in MPa was recorded. A Nikon LV100ND light microscope was then used to determine the failure mechanism. Eight measurements were carried out for each sample type. A FEI Quanta 650 microscope equipped with an Oxford Instruments X-Max -150 EDX Detector was used for elemental mapping of the pull off stubs.

### 2.4. Electrical testing

#### 2.4.1. AFM dielectric breakdown measurements

Atomic Force Microscopy (AFM) was utilised to measure the dielectric breakdown of the films as deposited onto copper disks. This was carried using an Oxford Instruments Cypher S equipped with a high voltage module and an Asylum Research ASYELEC.01 Ti/Ir coated tip [31]. Measurements were carried out by generating a 30 × 30 μm topographic image (in tapping mode) and then a grid of 4 × 4 locations was used on top of the image. At each location a voltage ramp (0–150 *V* at a rate of 37.5 $Vs^{-1}$) was applied to the copper substrate until a sharp increase in current was detected through the probe.

## 3. Results

### 3.1. Structural characterisation

FTIR spectra for RF sputtered $SiO_2$ shows peaks resulting from Si—O bonds at 1151 and 807 $cm^{-1}$. RF $Ta_2O_5$ spectra displayed a broad absorbance band with peaks at 745 and 890 $cm^{-1}$. Multilayer composites contained a spectra resulting from the superimposition of these peaks with an Al—O LO phonon vibration peak at *ca.* 900 $cm^{-1}$. The $SiO_2$ composites display an additional peak at 1229 $cm^{-1}$. All peaks for RF films and composites have been identified in Fig. 2a. Diffraction patterns (see Fig. 2b) showed the X-ray amorphous nature of all of the films, suggested by broad diffraction associated with an amorphous hump, which resulted from contributions from both the film and amorphous glass substrate. In the case of RF $Ta_2O_5$, two broad

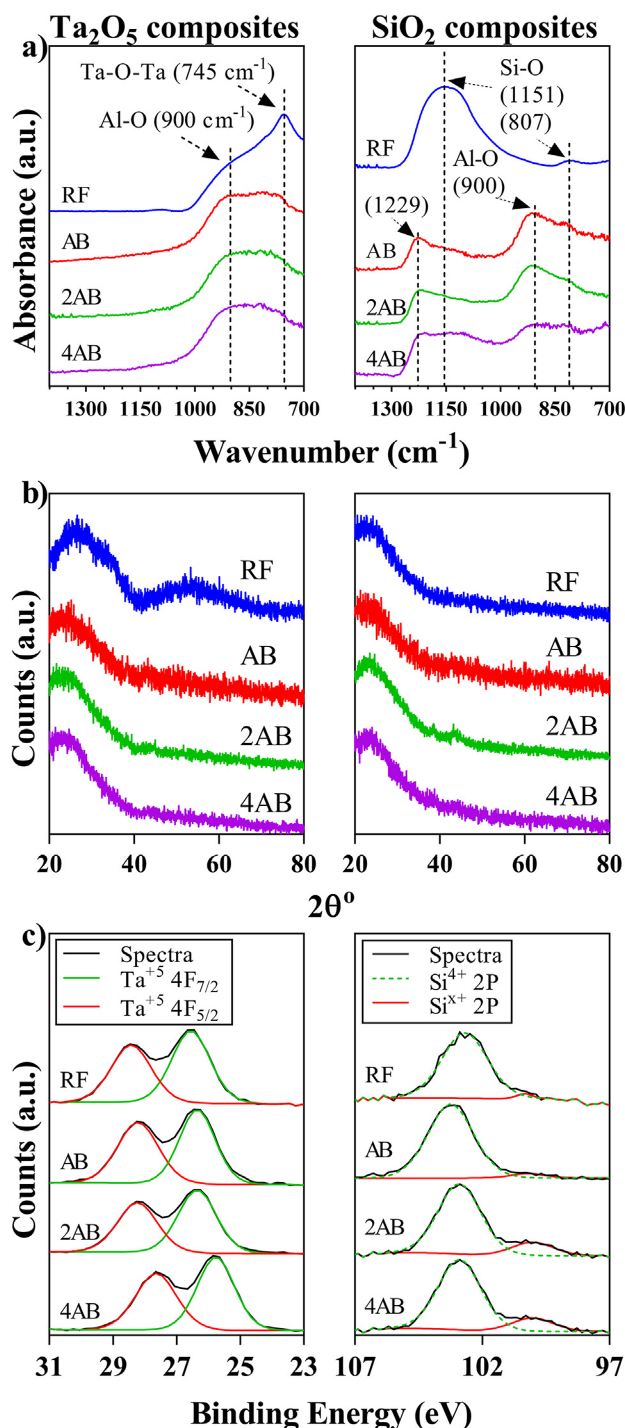


**Fig. 2.** a) FTIR spectra for $Ta_2O_5$ and $SiO_2$ composites as deposited onto copper foil. The main absorbance bands and their assignments have been indicated. b) shows XRD diffraction patterns for $Ta_2O_5$ and $SiO_2$ composites as deposited onto glass coverslips, indicating the films amorphous nature. c) XPS peak deconvolution for $Ta_2O_5$ and $SiO_2$ composites (as deposited onto Cu disks, identity of the peaks fitted are indicated).

amorphous humps can be seen which correlate to amorphous $Ta_2O_5$.

XPS spectra gave the stoichiometry and binding energies of the top 5 nm layer of the films. Binding energies of 26.3 ± 0.1 eV were observed for Ta_4F photoelectrons, whereas binding energies of 103.2 ± 0.1 eV were observed for Si_2P photoelectrons with a shoulder at 100.5 ± 0.1 eV, see Fig. 2c and Table 2. The amount of non-stoichiometric silicon calculated from the Si peak was seen to increase with an increasing number of layers. Yielding a transition from 1.9 to 16.1% between AB and 4AB composites. The Si:O ratios for the films varied between 0.43 and 0.62 where the ideal Si:O is 0.5. No peaks were found in the $Ta_2O_5$ composite spectra resulting from $Ta^0$ and the Ta:O ratios were generally consistent between, 0.35 and 0.4 where the ideal ratio is 0.4.

Deconvolution of the O_1S peak for the $SiO_2$ composites gave information as to the binding energy and composition of the Si species, see Table 3 for the oxygen binding energies and percentages determined by deconvolution.

Cross-sectional SEM imaging was used to show film thickness for use in the dielectric breakdown strength calculations. Layers could not be distinguished in most cases due to limiting resolution of the instrument and similar appearance, however, using backscattered imaging for $Ta_2O_5$ composites some layer structure could be seen in AB and 2AB films (the light areas can be seen resulting from the high molecular weight *ca.* 181 g mol$^{-1}$ Ta atoms) as seen along with sample thickness in Fig. 3 and Table 4. All films appeared to be predominately featureless. The layers in $SiO_2$ composite films were not clearly observed in backscattered or secondary electron mode (see Fig. 3).

**Table 2**
XPS Ta_4F and Si_2P binding energies, elemental ratios and oxidation states for composite films as deposited onto Cu disks.

| | Layer config. | $Ta^{5+}$_4F (eV) | $Ta^0$_4F (eV) | $Ta^0$% | Ta:O ratio |
|---|---|---|---|---|---|
| $Ta_2O_5$ | RF | 26.3 | N/A | N/A | 0.39 |
| | AB | 26.2 | N/A | N/A | 0.35 |
| | 2AB | 26.3 | N/A | N/A | 0.39 |
| | 4AB | 26.2 | N/A | N/A | 0.40 |
| | Layer config. | $Si^{4+}$_2P (eV) | $Si^{1+}$_2P (eV) | $Si^{1+}$ % | Si:O ratio |
| $SiO_2$ | RF | 103.2 | 100.8 | 3.5 | 0.43 |
| | AB | 103.2 | 100.2 | 1.9 | 0.62 |
| | 2AB | 103.2 | 100.2 | 4.4 | 0.58 |
| | 4AB | 103.2 | 100.3 | 16.1 | 0.56 |

### 3.2. Electrical testing

Dielectric breakdown measurements revealed a range of breakdowns for the multilayer materials. The highest dielectric strength was observed in both the case of $Ta_2O_5$ and $SiO_2$ composites where the 2AB motif was used, at 513 and 466 Vμm$^{-1}$ respectively. The lowest dielectric strength was seen in AB films at 332 and 350 Vμm$^{-1}$ for $SiO_2$ and $Ta_2O_5$ respectively.

The standard error in the voltage measurements was at least four times lower for $Ta_2O_5$ films as seen in Table 4, the error in AB films was also highest for each set of materials as seen in Table 4 and Fig. 4. The maximum leakage current prior to breakdown was determined using the current applied field plots and was shown to be up to *ca.* 60 times larger in the $Ta_2O_5$ composites, with maximum leakages of *ca.* 6.48, 3.13 and 2.35 nA (AB, 2AB, 4AB) whilst leakage prior to breakdown was < 0.1 nA in all $Al_2O_3$-$SiO_2$ composite films. Oscillations in the current leakage prior to breakdown were also seen in $Ta_2O_5$ composites but not in $SiO_2$ composites, see Fig. 4b.

**Table 3**
Binding energies and contribution of Si in the O_1S high resolution spectra from $SiO_2$ composites as deposited onto Cu disks.

| Layer config. | $Si^{4+}$ | | Shoulder 1 | | Shoulder 2 | |
|---|---|---|---|---|---|---|
| | (eV) | % | (eV) | % | (eV) | % |
| RF | 532.6 | 68.8 | 534.6 | 29.1 | 531.6 | 2.1 |
| AB | 532.5 | 93.9 | 534.5 | 3.4 | 530.2 | 2.6 |
| 2AB | 532.6 | 91.2 | 534.5 | 5.1 | 530.8 | 3.7 |
| 4AB | 532.56 | 93.6 | 534.5 | 4.4 | 530.7 | 2.2 |

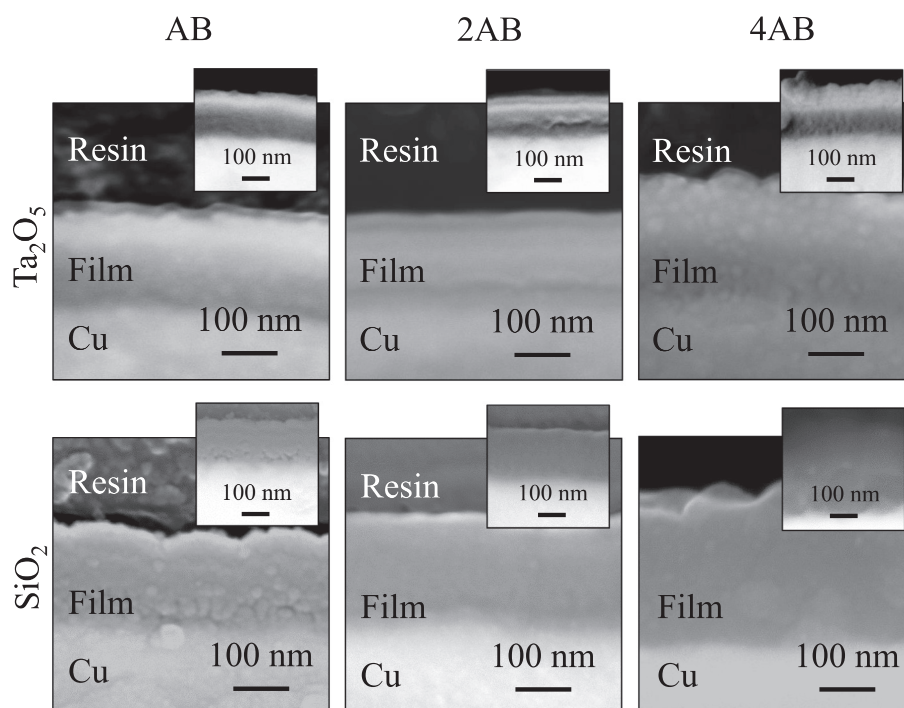


**Fig. 3.** Secondary and back scattered (inset) Cross sectional SEM of composite films $Ta_2O_5$ (top) and $SiO_2$ (bottom) as deposited onto Cu disks and mounted in resin. Average film thickness are displayed in Table 4.

**Table 4**
Breakdown voltage and dielectric breakdown for $Ta_2O_5$ and $SiO_2$ multilayer composites as deposited onto Cu disks. Layer structure and overall film thickness has been included (and was used to calculate the dielectric strength).

| | Layer config. | Thickness (nm) | Breakdown AVG. (V) | Error (V) | N | Dielectric Strength (Vμm$^{-1}$) |
|---|---|---|---|---|---|---|
| $SiO_2$ | AB | 191 ± 4 | 63.4 | 30.4 | 16 | 332 |
| | 2AB | 182 ± 4 | 84.9 | 15.6 | 16 | 466 |
| | 4AB | 236 ± 11 | 98.3 | 16.5 | 16 | 416 |
| $Ta_2O_5$ | AB | 203. ± 6 | 71.0 | 7.5 | 16 | 350 |
| | 2AB | 152 ± 4 | 78.0 | 2.1 | 16 | 513 |
| | 4AB | 210 ± 9 | 84.6 | 4.1 | 16 | 403 |

### 3.3. Mechanical testing

Pull off testing carried out on the multilayer composite films showed that the adhesive strength varied between 11.4 ± 1.8 and 34.3 ± 4.4 MPa with failure occurring through complete interfacial delamination and partial interfacial delamination between the coating and the substrate for all of the films. Average pull off values and failure mechanisms for each film are given in Table 5.

It can be seen that $Ta_2O_5$ composites produced with an AB layer configuration had a larger adhesion strength than the other $Ta_2O_5$ composites by *ca.* 1.5 times. Whilst the highest adhesion seen in $SiO_2$ composites was for the 4AB layer structure. EDX of the pull off stubs revealed a layer of copper on tested samples indicating that failure occurred at the initial Cu—Cu interface (see Fig. 5).

## 4. Discussion

The deposition of amorphous thin $SiO_2$ and $Ta_2O_5$ composites using RF power was shown to be possible with FTIR (showing bonding peaks for each component of the films) and XPS which confirmed the expected bonding configurations and desired compositional stoichiometry for the surface layers of the composites (see, Fig. 2). These materials were combined with PDC $Al_2O_3$, as deposited previously with a view to improving the dielectric strength above 310 Vμm$^{-1}$ [8]. RF sputtered $SiO_2$ and $Ta_2O_5$ both have the potential to have high breakdown strength as reported in the literature (higher than that achieved for pulsed DC alumina alone 570 and 600 Vμm$^{-1}$ respectively) making them ideal candidates for the multicomponent films [19,25]. The use of multi-layers is attractive because of the potential for suppression of charge transfer as explored by *Mackey* et al. for extruded polymer films [32]. The changes in mechanical and electrical properties will be discussed in the following section.

### 4.1. Structural

For the composite films multiple infrared absorption peaks associated with the composites constituent layers were seen, see Fig. 2. For $Ta_2O_5$ composites a broad absorbance peak resulted from Al—O phonon vibrations combined with $Ta_2O_5$ peaks at *ca.* 785 cm$^{-1}$ The $Ta_2O_5$ peak decreased in intensity from 0.97 to 0.92 a.u. with respect to the peak at *ca.* 820 cm$^{-1}$ as the $Ta_2O_5$ RF surface layer decreased in thickness. The decreasing layer thickness resulting in a diminished absorption peak, Ta-O-Ta peaks were similarly observed by *Mannequin* et al. in electron beam evaporated and sputtered films [22].

The FTIR spectra of $SiO_2$ composites had overlapping Al—O and Si—O peaks, similar combinations of peaks - resulting from $Al_2O_3$ and $SiO_2$ vibrations and Al-O-Si linkages - were seen in heat treated $Al_2O_3$-$SiO_2$ composite aerogels produced by *Wu* et al. [33]. Hence assignment of the peak at 1229 cm$^{-1}$ was to either Al-O-Al bonding or Al-O-Si bonding. This could suggest Al-O-Si bonding at the $Al_2O_3$, $SiO_2$ interfaces, which may lead to improved adhesion [34].

Discrete layers were too thin to be imaged using SEM techniques, as seen in Fig. 3. The XRD pattern for RF $Ta_2O_5$ was not replicated in multi-layer $Ta_2O_5$ films, this was because the sample used to measure the RF properties was deposited to 774 nm whilst the $Ta_2O_5$ layers in the composites had a total and maximum thickness of 50 nm which resulted in the single amorphous hump, due to a lack of instrument

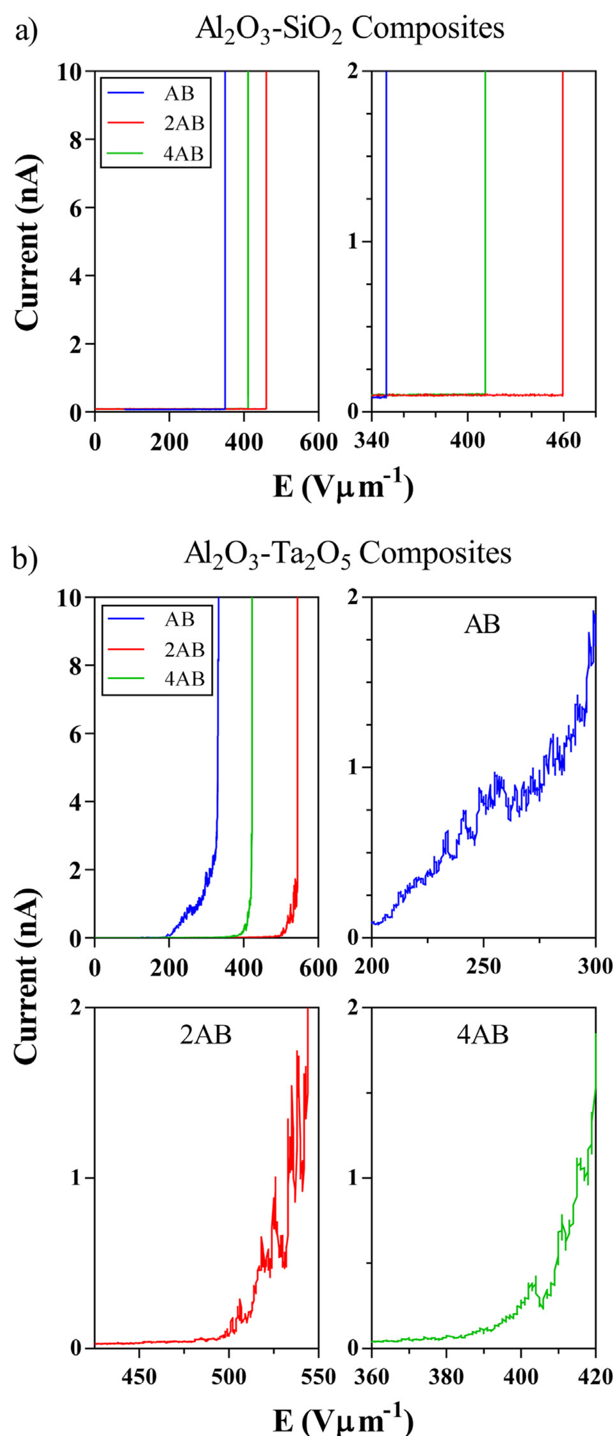


**Fig. 4.** AFM measurement of current, applied field plots indicating the onset of breakdown and current leakage prior to breakdown. a) Plots for $SiO_2$ composites, including a high resolution graph showing the low leakage current (< 0.1 nA) prior to breakdown. b) Plots for $Ta_2O_5$ composites which Includes high resolution graphs showing current oscillation associated with charge trapping and de trapping, prior to break down. For both materials the layer configuration is indicated in the key.

sensitivity.

All the RF layers used for the 4AB composites had a thickness in excess of the XPS penetration depth such that all the photo electrons originated from the surface of the top layers of $Ta_2O_5$ or $SiO_2$. For the $Al_2O_3$-$SiO_2$ composites XPS determined that the level of $Si^{1+}$ increased in every instance where the number of layers was increased, hence the

**Table 5**
Average adhesive pull off strength (MPa) and failure mechanism for $Ta_2O_5$ and $SiO_2$ multilayer films as deposited onto Cu disks.

| | Sample | Average failure strength (MPa) | Complete interfacial failure | Partial interfacial failure | Failure in Adhesive |
|---|---|---|---|---|---|
| $Ta_2O_5$ | AB | 24.6 ± 3.1 | 4 | 3 | 0 |
| | 2AB | 16.0 ± 2.2 | 8 | 0 | 0 |
| | 4AB | 15.3 ± 2.8 | 8 | 0 | 0 |
| $SiO_2$ | AB | 22.0 ± 3.4 | 6 | 2 | 0 |
| | 2AB | 11.4 ± 1.8 | 8 | 0 | 0 |
| | 4AB | 34.3 ± 4.4 | 1 | 7 | 0 |

layers decreased in thickness. Deconvolution of the O_1S peaks (not shown) was used to determine the identity of the $Si^{1+}$ species. This analysis showed that the $Si^{1+}$ shoulders were made up of contributions from surface hydroxides at 534.5 ± 0.1 eV accounting for between 2.1 and 3.7% and $SiO_{2-X}$ species at 530.6 ± 0.2 eV accounting for between 3.4 and 5.1%. The amount attributed to $SiO_{2-X}$ species was lower than the 29.1% seen for RF films [35]. This improvement – with respect to the level of $SiO_{2-X}$ in RF films - is attributed to target conditioning during reactive PDC $Al_2O_3$ sputtering as well as the decreased sputtering time [36]. These parameters combined to decrease the effect of preferential sputtering on the film composition. This, however, cannot account for the large increase in the $Si^{1+}$ shoulder seen for 4AB films. The lack of Al_2P photo electrons in the survey spectra rules out the influence of compound material at the boundaries (such as Al-O-Si as suggested by FTIR) on the XPS results, thus the amount of $Si^{1+}$ in the films. This is therefore likely a result of the increase in total sputtering time (when considering the multiple blending stages required for the 4AB films) resulting in preferential sputtering effects, which increased the amount of compositional defects.

Conversely, the $Al_2O_3$-$Ta_2O_5$ films emitted only $Ta^{5+}$ photoelectrons and had stoichiometry which varied between a Ta:O ratio 0.35 and 0.4, as seen in Table 2. Thus it is likely that conditioning stages during PDC sputtering was sufficient to produce stoichiometric $Ta_2O_5$ films. Deconvolution of the O1_S peak in this case yielded two peaks similarly to work by *Mannequin* et al. who showed the possibility of the peak resulting from O—H, oxygen vacancies or O—C from contaminants or surface species [22,37].

### 4.2. Electrical characterisation

Dielectric breakdown measurements of the composite films showed a significant improvement in the dielectric strength of 2AB and 4AB composites, resulting in a minimum increase of 93 ± 37 Vμm$^{-1}$ compared to PDC $Al_2O_3$ alone, whilst the difference between the AB and PDC films was insignificant. The improvements in 2AB and 4AB composites are likely a result of barrier properties of the inserted layers, whereby they inhibit the flow of current through defect sites within the films, meaning that charge transit through the thickness of the material occurs at a higher applied field. Barrier effects have been studied for solid polymer dielectrics by *Gefle* et al. who discussed a mechanism by which material interfaces prevent charge propagation across films improving the dielectric strength [12]. Other work which implemented clay modification of polymers was shown to improve dielectric strength by up to 17.2% [38,39]. The improvement was attributed to the suppression of charge injection and migration, which resulted in the inhibition of an electron cascade. Interestingly, bi-axially orientated polypropylene only showed marginal improvements (1.1%) because of its intrinsic dielectric strength. *Mattox* also noted that multilayers can be useful for decreasing the number of pinholes resulting from abnormalities during growth [40].

Taking this research into account it can be seen that incorporating

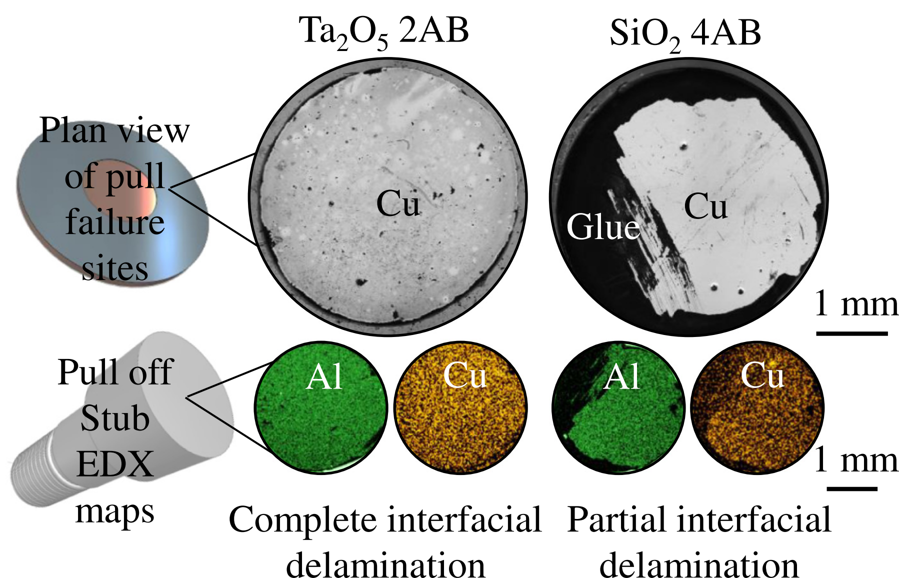


**Fig. 5.** Example images of complete and partial delamination sites, for $Ta_2O_5$ 2AB (left) and $SiO_2$ 4AB (right) respectively. Below each light micrograph are the EDX maps of the pull off stub for Cu and Al, which indicate that the failure was at the Cu substrate interface.

barrier layers with a higher dielectric strength relative to the base material has the potential to increase the breakdown strength and lower leakage current. It is suggested that the mechanisms for the improvement in $SiO_2$ and $Ta_2O_5$ composites include: capping structural and compositional defects, prevention of charge injection and disrupting the growth of breakdown channels. The work by *Ren* et al. showed materials with sufficient intrinsic breakdown strength were not affected by layering, thus the RF deposition method is seen as key to producing films with high enough breakdown voltage to act as sufficient barrier layers in the PDC $Al_2O_3$.

In ceramic multilayers produced by *Martinez-Perdiguero* et al. a two times improvement in the dielectric strength of sputtered $SiO_2$-$Al_2O_3$ composite coatings was noted, giving a maximum of 80 $V\mu m^{-1}$. This condition was met when transitioning from single layer $Al_2O_3$ into 2,4 and 8 layer composite materials [20]. Improvements of this kind could be the result of added layers masking structural or compositional defects, such as in the $Al_2O_3$-$SiO_2$ gas diffusion barrier films, produced using ALD by *Dameron* et al. [13]. AFM is a powerful tool which has the capability of generating dielectric breakdown measurements and current voltage data which can be used to determine leakage current. This method allows high spatial resolution in a well-defined array avoiding the effect of making multiple measurements too close to one another and allowing the avoidance of extrinsic defects. AFM has been used to measure the dielectric strength of thin films by *Ganesan* et al. and even to perform layer by layer breakdown testing on BN by *Hattori* et al. [41,42]. However, AFM dielectric breakdown measurements have not been widely used for multilayer ceramic films past the BN films mentioned above.

$Ta_2O_5$ composites had a higher maximum dielectric strength of 513 ± 18 $V\mu m^{-1}$ than the $SiO_2$ composites where the maximum was 466 ± 86 $V\mu m^{-1}$ (see Fig. 4). There was, however, a large difference in the conduction prior to breakdown with higher current leakage and large oscillations seen in $Ta_2O_5$ composites resulting from charge trapping and de-trapping. The higher the leakage current the worse the dielectric is at preventing current flow; which is the primary purpose for these films. Larger levels of leakage current are symptomatic of defects in the film, which are capable of facilitating charge transfer. These oscillations caused by charge trapping and de-trapping, which can be caused by intrinsic or electrical stress induced defects, were noticeably more sever in $Ta_2O_5$ AB composites. Such oscillations were also seen in reactively sputtered $Al_2O_3$ films as measured by AFM techniques [8,42]. The maximum current flow prior to breakdown was *ca.* 6 and 0.1 nA for $Ta_2O_5$ and $SiO_2$ composites respectively. This shows that the RF $SiO_2$ acted as a superior barrier layer than the RF $Ta_2O_5$. The lack of observable oscillations in the $SiO_2$ composites suggests that the $SiO_2$ layers contained fewer defects capable of trapping charge and were not susceptible to stress induced leakage current, which could also cause charge trapping and de-trapping [42].

The $Ta_2O_5$ and $SiO_2$ 2AB layer composites produced the films with the highest dielectric strengths. This is likely due to a compromise between layer thickness and frequency of the barrier layers; given that films were all deposited to < 236 nm. The barrier frequency in AB films was insufficient and the thickness of the RF layer in 4AB films was too thin to offer as effective barrier effects (the RF layer is half as thick as the 2AB sample). Such layer dependence was seen in $HfO_2$ $Al_2O_3$ composites produced by *Park* et al. where composites with 7 and 5 layers had enhanced breakdown characteristics compared to 3 layer materials; this phenomena was attributed the $Al_2O_3$ layers blocking the current between grain boundaries in the $HfO_2$ layers [43]. The poorer electrical properties in the $SiO_2$ 4AB composites could also be the result of apparent increased amount of sub $Si^{4+}$ silicon from 1.9 to 15.8% at the surface of the $SiO_2$ composite films as identified in the XPS in Fig. 6.

### *4.3. Mechanical characterisation*

The pull off adhesion strengths of all of the composites were shown to be on average 2.4 times lower than that of the solely PDC alumina films which had an average failure strength of 55.7 ± 2.9 MPa [8]. The failure also shifted from predominantly partial interfacial failure to complete interfacial failure (in this study, see Fig. 5). The substrates in both cases were treated using the same methods, thus the decrease must be ascribed to the use of multilayers, due to the use of dissimilar materials in the films. It could therefore be the case that the implementation of multilayers resulted in a higher level of intrinsic stress, which would result in this decrease in adhesion. Intrinsic stress in PVD thin films originate from either variation in thermal expansion between the substrate and the films or from growth induced stresses produced during condensation [44]. *Knotek* et al. have explored the effect of PVD deposition techniques on intrinsic stress, showing the dramatic effect of processing parameters, achieving a 1 GPa reduction of growth induced compressive stress by applying substrate heating [44]. For instance a two fold increase in film adhesion strength was seen when decreasing

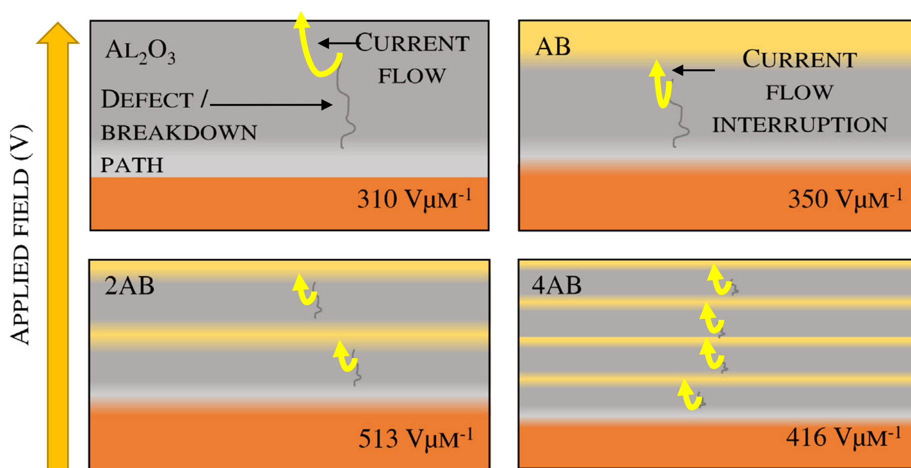


**Fig. 6.** Effect of multilayers in capping defects and improving barrier properties, by resisting current flow and disrupting the breakdown path. Defects are shown to be passivated in films with multilayer configuration and the dielectric strength is highest for the 2AB films. The maximum dielectric strength for each layer configuration is given in the bottom right of each illustration.

the intrinsic stress from $4.84 \times 10^{-9}$ to $0.21 \times 10^{-9}$ Pa by chopping in *ca.* 180–200 nm $CeO_2$ films deposited by *Patil* et al., who also showed the same effect in ZnS films [45,46]. The use of interlayers also increased intrinsic stress in multilayer $BaTiO_3$/Ni ceramic capacitors, analysed by *Park* et al. [11,47]. An increase in the $BaTiO_3$/Ni layer frequency increased the compressive in plane stress, which reached a maximum at < 135 MPa compressive stress. Complete interfacial failure at the Cu—Cu interface occurred at all test sites in the current study, which indicates that the blending stages were sufficient to mitigate cohesive failure between the sputtered layers. Blending stages have been used extensively for improving the adhesion of diamond like carbon films. For instance, a number of graded layers (such as TiC) can be used to avoid detachment and high interfacial stresses. This is achieved through a gradation of the thermal expansion coefficient ($8.6 \times 10^{-6}$ to $6.2 \times 10^{-6}$ to $1.0 \times 10^{-6}$ °C$^{-1}$ for Ti, TiC and DLC respectively). Gradation of this kind can also decrease lattice mismatches, such as in the Ti-TiC-DLC system by transitioning through a number of intermediate mixed structures from the dominant hcp phase of Ti to fcc for TiC [48–50]. It was also shown by *Pei* et al. that graded interfaces in ZrCu/Cu multi-layered films improved mechanical properties (elastic modulus, tensile yield stress and tensile elongation increased by a minimum of 1.3 times for 8 to 10 layer films), compared to sharp interfaces because of the reduced stress and mismatches at the interfaces [51].

There was no significant difference in the average adhesion strength of the $Ta_2O_5$ and $SiO_2$ composites in the case of the AB and 2AB conformers, with pull off adhesion averages of 20.3 ± 3.8 and 16.7 ± 4.4 MPa for $Ta_2O_5$ and $SiO_2$ composites respectively. $SiO_2$ 4AB composites did, however, have superior maximum pull off adhesion over the equivalent $Ta_2O_5$ composites, as the average pull off adhesion attests: 34.3 ± 4.4 and 15.3 ± 2.8 MPa respectively. The coefficients of thermal expansion were reported to be $5.4 \times 10^{-6}$, $5.1 \times 10^{-7}$ and $3.6 \times 10^{-6}$ °C$^{-1}$ for sputtered $Al_2O_3$, $SiO_2$ and $Ta_2O_5$ respectively [52]. Thus the decrease in properties when using $Ta_2O_5$ in the 4AB composites was a direct result of the larger thermal expansion coefficient; which led to an increase in internal stress within the composites upon cooling from the processing temperature. Generally a decrease in properties was seen when transitioning to 2AB and 4AB films from AB films (Table 5) suggesting an increase in internal stress with an increasing number of layers and interfaces.

Combining PDC $Al_2O_3$ with RF sputtered multilayers has been shown to be beneficial when regarding the dielectric strength of thin films, through a combination of defect capping and disruption of breakdown paths. Whilst the adhesive properties suffered, development of a more comprehensive interlayer system could allow these coatings to be used as insulation for wires or micro electrical components.

## 5. Conclusions

AFM dielectric breakdown data displayed in this work has shown the electrical breakdown potential for multilayer films consisting of pulsed DC sputtered $Al_2O_3$ and a RF sputtered $SiO_2$ or $Ta_2O_5$ layers to have improved breakdown strength compared to those of pulsed DC $Al_2O_3$ alone. This was attributed to barrier effects and the requirement for charge carriers to travel across layer interfaces. The best layer configuration was seen to be the 2AB motif, which offered the best compromise between layer thickness and number of layers. Leakage current in $SiO_2$ composites was a maximum of 60 times lower than that of the $Ta_2O_5$ composites prior to breakdown. $SiO_2$ was shown to act as a better barrier layer preventing the flow of current more effectively prior to breakdown. The mechanical testing showed that the blending stages used during film production were sufficient to prevent cohesive failure between the various layers. However, the use of the multilayer systems was shown to decrease the adhesive properties of the films when compared to PDC $Al_2O_3$ alone by a minimum of two times with respect to pull off adhesion.

## Acknowledgements

The authors would like to thank the Nanoscale and Microscale Research Centre (nmRC) for providing access to instrumentation. This work was supported by the Engineering and Physical Sciences Research Council [grant number EP/LO22494/1]. The authors also wish to acknowledge the support of the beacon in Propulsion Futures and the Institute for Aerospace Technology at the University of Nottingham.

## References


[1] A.X. Wei, Z.X. Ge, X.H. Zhao, J. Liu, Y. Zhao, Electrical and optical properties of tantalum oxide thin films prepared by reactive magnetron sputtering, J. Alloys Compd. 509 (2011) 9758–9763.
[2] C. Besleaga, G.E. Stan, I. Pintilie, P. Barquinha, E. Fortunato, R. Martins, Transparent field-effect transistors based on AlN-gate dielectric and IGZO-channel semiconductor, Appl. Surf. Sci. 379 (2016) 270–276.
[3] J.-C. Marè, J. Fu, Review on signal-by-wire and power-by-wire actuation for more electric aircraft, Chin. J. Aeronaut. 30 (2017) 857–870.
[4] V. Madonna, P. Giangrande, M. Galea, Electrical power generation in aircraft: review, challenges, and opportunities, IEEE Trans. Transp. Electrif. 4 (2018) 646–659.
[5] J. Beatty, An Advanced Arc Track Resistance Airframe Wire, St. Augustine, (1995).
[6] F.C. Carreri, R. Bandorf, H. Gerdes, M. Vergöhl, G. Bräuer, Highly insulating alumina films by a bipolar reactive MF sputtering process with special arc handling, Surf. Coat. Technol. 290 (2016) 82–86.
[7] H. Bartzsch, D. Glöß, B. Böcher, P. Frach, K. Goedicke, Properties of $SiO_2$ and $Al_2O_3$ films for electrical insulation applications deposited by reactive pulse magnetron sputtering, Surf. Coat. Technol. 174 (2003) 774–778.
[8] B.V.T. Hanby, B.W. Stuart, C. Grant, J. Moffat, J. Blissett, C. Gerada, M. Gimeno-Fabra, D.M. Grant, Dielectric breakdown of alumina thin films produced by pulsed direct current magnetron sputtering, Thin Solid Films 662 (2018) 145–154.
[9] B. Peng, D. Gong, W. Zhang, J. Jiang, L. Shu, Y. Zhang, Effects of sputtering

parameters on AlN film growth on flexible hastelloy tapes by two-step deposition technique, Materials (Basel) 9 (2016) 1–9.
[10] D. Miao, H. Hu, A. Li, S. Jiang, S. Shang, Fabrication of porous and amorphous $TiO_2$ thin films on flexible textile substrates, Ceram. Int. 41 (2015) 9177–9182.
[11] J.S. Park, S. Kim, H. Shin, H.S. Jung, K.S. Hong, Residual stress evolution in multilayer ceramic capacitors corresponding to layer increase and its correlation to the dielectric constant, J. Appl. Phys. 97 (2005) 1–5.
[12] O.S. Gefle, S.M. Lebedev, V.Y. Uschakov, The mechanism of the barrier effect in solid dielectrics, J. Phys. D. Appl. Phys. 30 (1997) 3267–3273.
[13] A.A. Dameron, S.D. Davidson, B.B. Burton, P.F. Carcia, R.S. Mclean, S.M. George, Gas diffusion barriers on polymers using multilayers fabricated by $Al_2O_3$ and rapid $SiO_2$ atomic layer deposition, J. Phys. Chem. C 112 (2008) 4573–4580.
[14] K. Chu, Y.G. Shen, Mechanical and tribological properties of nanostructured TiN/TiBN multilayer films, Wear 265 (2008) 516–524.
[15] P. Zou, M. Yao, J. Chen, Y. Peng, X. Yao, Leakage current and dielectric breakdown in lanthanum doped amorphous aluminum oxide films prepared by sol–gel, Ceram. Int. 42 (2016) 4120–4125.
[16] S.-H. Jeong, J.-K. Kim, B.-S. Kim, S.-H. Shim, B.-T. Lee, Characterization of $SiO_2$ and $TiO_2$ films prepared using rf magnetron sputtering and their application to anti-reflection coating, Vacuum 76 (2004) 507–515.
[17] B. Stuart, M. Gimeno-Fabra, J. Segal, I. Ahmed, D.M. Grant, Preferential sputtering in phosphate glass systems for the processing of bioactive coatings, Thin Solid Films 589 (2015) 534–542.
[18] L.-N. He, J. Xu, Properties of amorphous $SiO_2$ films prepared by reactive RF magnetron sputtering method, Vacuum 68 (2002) 197–202.
[19] S.-I. Jun, T.E. McKnight, A.V. Melechko, M.L. Simpson, P.D. Rack, Characterisation of reactively sputtered silicon oxide for thin-film transistor fabrication, Electron. Lett. 41 (2005) 1–2.
[20] J. Martínez-Perdiguero, L. Mendizabal, M.C. Morant-Miñana, I. Castro-Hurtado, A. Juarros, R. Ortiz, A. Rodriguez, Electrical insulation and breakdown properties of $SiO_2$ and $Al_2O_3$ thin multilayer films deposited on stainless steel by physical vapor deposition, Thin Solid Films 595 (2015) 171–175.
[21] M. Putkonen, P. Sippola, L. Svärd, T. Sajavaara, J. Vartiainen, I. Buchanan, U. Forsström, P. Simell, T. Tammelin, Low-temperature atomic layer deposition of $SiO_2/Al_2O_3$ multilayer structures constructed on self-standing films of cellulose nanofibrils, Philos. Trans. R. Soc. A Math. Phys. Eng. Sci. 376 (2018) 1–12.
[22] C. Mannequin, T. Tsuruoka, T. Hasegawa, M. Aono, Identification and roles of nonstoichiometric oxygen in amorphous $Ta_2O_5$ thin films deposited by electron beam and sputtering processes, Appl. Surf. Sci. 385 (2016) 426–435.
[23] C. Chaneliere, J.L. Autran, R.A.B. Devine, B. Balland, Tantalum pentoxide ($Ta_2O_5$) thin films for advanced dielectric applications, Mater. Sci. Eng. R 22 (1998) 269–322.
[24] G.S. Oehrlein, A. Reisman, Electrical properties of amorphous tantalum pentoxide thin films on silicon, J. Appl. Phys. 54 (1983) (6502–2538).
[25] S. Seki, T. Unagami, O. Kogure, B. Tsujiyama, Formation of high-quality, magnetron-sputtered $Ta_2O_5$ films by controlling the transition region at the $Ta_2O_5$/Si interface, Cit. J. Vac. Sci. Technol. A. 5 (1987) 1771–1774.
[26] S.W. Smith, K.G. McAuliffe, J.F. Conley, Atomic layer deposited high-k nanolaminate capacitors, Solid State Electron. 54 (2010) 1076–1082.
[27] K. Ganesan, S. Ilango, S. Mariyappan, M. Farrokh Baroughi, M. Kamruddin, A.K. Tyagi, Conductive atomic force microscopy studies on dielectric breakdown behavior of ultrathin Al2O3 films, Appl. Phys. Lett. 98 (2011) 1–3.
[28] S. Kremmer, C. Teichert, E. Pischler, H. Gold, F. Kuchar, M. Schatzmayr, Characterization of silicon gate oxides by conducting atomic force microscopy, Surf. Interface Anal. 33 (2002) 168–172.
[29] A. Ando, K. Miki, K. Sakamoto, Conducting-AFM studies on local dielectric breakdown of ultrathin SiO2 films, in: Ext. Abstr. Int. Work. Gate Insul. IWGI 2001 (IEEE Cat. No.01EX537), Japan Soc. Appl. Phys (2001) 124–126.
[30] A.I. Abdulagatov, Y. Yan, J.R. Cooper, Y. Zhang, Z.M. Gibbs, A.S. Cavanagh, R.G. Yang, Y.C. Lee, S.M. George, $Al_2O_3$ and $TiO_2$ atomic layer deposition on copper for water corrosion resistance, ACS Appl. Mater. Interfaces 3 (2011) 4593–4601.
[31] Asylum Research, AFM Tools for Nanoscale Electrical Characterization, (2018).
[32] M. Mackey, A. Hiltner, E. Baer, L. Flandin, M.A. Wolak, J.S. Shirk, Enhanced breakdown strength of multilayered films fabricated by forced assembly microlayer coextrusion, J. Phys. D. Appl. Phys. 42 (2009) 1–12.
[33] X. Wu, G. Shao, S. Cui, L. Wang, X. Shen, Synthesis of a novel $Al_2O_3$–$SiO_2$ composite aerogel with high specific surface area at elevated temperatures using inexpensive inorganic salt of aluminum, Ceram. Int. 42 (2016) 874–882.
[34] L.A.S.A. Prado, M. Sriyai, M. Ghislandi, A. Barros-Timmons, K. Schulte, Surface modification of alumina nanoparticles with silane coupling agents, J. Braz. Chem. Soc. 21 (2010) 2238–2245.
[35] J.W. Ma, W.J. Lee, J.M. Bae, K.S. Jeong, S.H. Oh, J.H. Kim, S.H. Kim, J.H. Seo, J.P. Ahn, H. Kim, M.H. Cho, Carrier mobility enhancement of tensile strained Si and SiGe nanowires via surface defect engineering, Nano Lett. 15 (2015) 7204–7210.
[36] C.S. Bhatia, Alumina films by sputter deposition with $Ar/O_2$: preparation and characterization, J. Vac. Sci. Technol. A Vacuum, Surfaces, Film. 7 (1989) 1298–1302.
[37] W. Hu, L. Zou, C. Gao, Y. Guo, D. Bao, High speed and multi-level resistive switching capability of $Ta_2O_5$ thin films for nonvolatile memory application, J. Alloys Compd. 676 (2016) 356–360.
[38] B. Zhang, Z. Li, M. Ren, J. Liu, T. Moran, B. Huey, L. Sun, Y. Cao, A superior nanolaminate dielectric barrier coating for high breakdown strength, 2017 IEEE Conf. Electr. Insul. Dielectr. Phenom, IEEE, 2017, pp. 461–464.
[39] M. Ren, J. Liu, L. Sun, Y. Cao, Enhancing dielectric property of polymer films with nanoclay coatings, 2016 IEEE Conf. Electr. Insul. Dielectr. Phenom, IEEE, 2016, pp. 651–654.
[40] D.M. Mattox, Adhesion and deadhesion, Handb. Phys. Vap. Depos. Process. (2010) 439–474.
[41] Y. Hattori, T. Taniguchi, K. Watanabe, K. Nagashio, Layer-by-layer dielectric breakdown of hexagonal boron nitride, ACS Nano 9 (2015) 916–921.
[42] K. Ganesan, S. Ilango, M. Shanmugam, M. Farrokh Baroughi, M. Kamruddin, A.K. Tyagi, Pre- and post-breakdown electrical studies in ultrathin $Al_2O_3$ films by conductive atomic force microscopy, Curr. Appl. Phys. 13 (2013) 1865–1869.
[43] I.S. Park, K.M. Ryu, J. Jeong, J. Ahn, Dielectric stacking effect of $Al_2O_3$ and $HfO_2$ in metal-insulator-metal capacitor, IEEE Electron Device Lett. 34 (2013) 120–122.
[44] O. Knotek, R. Elsing, G. Kramer, F. Jungblutt, On the origin of compressive stress in PVD coatings - an explicative model, Surf. Coat. Technol. 46 (1991) 265–274.
[45] P.V. Patil, R.K. Puri, V. Puri, Comparison of adhesion and intrinsic stress of chopped and non-chopped ZnS thin films, Mater. Chem. Phys. 49 (1997) 156–159.
[46] P.V. Patil, U.V. Nerle, V. Puri, R.K. Puri, Adhesion improvement and intrinsic stress decrease in cerium oxide thin films by chopping, J. Adhes. Sci. Technol. 10 (1996) 151–159.
[47] H. Shin, J.-S. Park, K. Sun Hong, H. Suk Jung, J.-K. Lee, K. Yop Rhee, Physical origin of residual thermal stresses in a multilayer ceramic capacitor influence of thickness and number of dielectric layers on residual stresses in micromultilayer ceramic capacitors, Cit. J. Appl. Phys. 101 (2007) 1–5.
[48] P.J. Kelly, R.D. Arnell, Magnetron sputtering: a review of recent developments and applications, Vacuum. 56 (1999) 159–172.
[49] A.A. Voevodin, M.A. Capano, S.J.P. Laube, M.S. Donley, J.S. Zabinski, Design of a Ti/TiC/DLC functionally gradient coating based on studies of structural transitions in Ti–C thin films, Thin Solid Films 298 (1997) 107–115.
[50] D.A. Outka, W.L. Hsu, D.R. Boehme, N.Y.C. Yang, D.K. Ottesen, H.A. Johnsen, T.J. Headley, W.M. Clift, Compilation of Diamond-like Carbon Properties for Barriers and Hard Coatings, Albequerque, (1994).
[51] H.J. Pei, S.Y. Kuan, M.C. Liu, J.C. Huang, Tensile behavior of amorphous/nanocrystalline ZrCu/cu multilayered films with graded interfaces, Intermetallics 31 (2012) 191–195.
[52] D.R.M. Crooks, G. Cagnoli, M.M. Fejer, G. Harry, J. Hough, B.T. Khuri-Yakub, S. Penn, R. Route, S. Rowan, P.H. Sneddon, I.O. Wygant, G.G. Yaralioglu, Experimental measurements of mechanical dissipation associated with dielectric coatings formed using $SiO_2$, $Ta_2O_5$ and $Al_2O_3$, Classical Quantum Gravity 23 (2006) 4953–4965.